

## A Sharp Look at Coronal Rain with *Hinode*/SOT and SST/CRISP

P. Antolin,<sup>1</sup> M. Carlsson,<sup>1</sup> L. Rouppe van der Voort,<sup>1</sup> E. Verwichte,<sup>2</sup> and G. Vissers<sup>1</sup>

<sup>1</sup>*Institute of Theoretical Astrophysics, University of Oslo, P.O. Box 1029, Blindern, NO-0315 Oslo, Norway*

<sup>2</sup>*Centre for Fusion, Space and Astrophysics, Department of Physics, University of Warwick, Coventry CV4 7AL, UK*

**Abstract.** The tropical wisdom that when it is hot and dense we can expect rain might also apply to the Sun. Indeed, observations and numerical simulations have showed that strong heating at footpoints of loops, as is the case for active regions, puts their coronae out of thermal equilibrium, which can lead to a phenomenon known as catastrophic cooling. Following local pressure loss in the corona, hot plasma locally condenses in these loops and dramatically cools down to chromospheric temperatures. These blobs become bright in  $H\alpha$  and  $\text{Ca II H}$  in time scales of minutes, and their dynamics seem to be subject more to internal pressure changes in the loop rather than to gravity. They thus become trackers of the magnetic field, which results in the spectacular coronal rain that is observed falling down coronal loops. In this work we report on high resolution observations of coronal rain with the Solar Optical Telescope (SOT) on *Hinode* and CRISP at the Swedish Solar Telescope (SST). A statistical study is performed in which properties such as velocities and accelerations of coronal rain are derived. We show how this phenomenon can constitute a diagnostic tool for the internal physical conditions inside loops. Furthermore, we analyze transverse oscillations of strand-like condensations composing coronal rain falling in a loop, and discuss the possible nature of the wave. This points to the important role that coronal rain can play in the fields of coronal heating and coronal seismology.

### 1. Introduction

There is now increasing evidence that active regions in the Sun have their heating concentrated mostly at lower atmospheric regions, from the lower chromosphere to the lower corona. The excess densities found in most observed coronal structures such as coronal loops put them out of hydrostatic equilibrium, a state that can be explained by basal heating (Aschwanden 2001). Hara et al. (2008), using the *Hinode*/EIS instrument, have shown that active region loops exhibit upflow motions and enhanced nonthermal velocities at their footpoints, fitting as well in the basal heating scenario. Recently, De Pontieu et al. (2011) have highlighted the importance of the link between the photosphere and the corona by showing that a considerable part of the hot coronal plasma gets heated at low spicular heights, thus explaining the fading character of the ubiquitous “type II spicules”. Further evidence of basal heating is put forward by the presence of cool structures in the active region coronae, such as filaments/prominences or coronal rain, two phenomena that are linked to the underlying magnetic field topology.

Both prominences (or filaments if observed on disk rather than at the limb) and coronal rain correspond to cool and dense plasma observed at coronal heights in chromospheric lines such as  $H\alpha$  and  $\text{Ca II H}$  and  $\text{K}$ . But while the plasma in prominences is suspended in the corona against gravity making the structures long-lived (days to weeks), coronal rain is observed falling down in timescales of minutes (De Groof et al. 2004; Schrijver 2001) along curved loop-like trajectories in the absence of prominences. It is generally agreed that the mechanical stability and thermodynamic properties of prominences are deeply linked to the underlying magnetic field topology, and thus we could think that the main difference with coronal rain is basically a difference on the magnetic field configuration in the corona. This is, however, a speculation that still needs to be addressed properly.

While prominences have been studied extensively in solar physics, coronal rain, on the other hand, is a phenomenon for which few observational studies exist, despite being observed since the early 1970s (Kawaguchi 1970; Leroy 1972). It is also generally believed to be a rather uncommon phenomenon of active region coronae. However, recent high resolution observations with instruments such as the CRISP Imaging Spectro-Polarimeter (CRISP) at the Solar Swedish Telescope (SST), the Solar Optical Telescope on *Hinode*, or the Solar Dynamics Observatory (SDO) are offering a different scenario in which coronal rain appears to be a rather ubiquitous phenomenon over active regions, a case which can have profound implications in coronal heating. Whether this is really the case will require further effort gathering a statistically significant number of observations in different wavelengths.

Numerical simulations have shown that coronal rain and prominences are most likely the result of a phenomenon of thermal instability, also known as 'catastrophic cooling'. Loops with basal heating present high coronal densities and thermal conduction turns out to be insufficient to maintain a steady heating per unit mass, leading to a gradual decrease of the coronal temperature. Eventually recombination of atoms takes place and temperature decreases to chromospheric values abruptly in a timescale of minutes locally in the corona. This is accompanied by local pressure losses leading to the formation of condensations which become bright or dark if observed towards the limb or on disk, respectively.

The catastrophic cooling leading to coronal rain is not due to a lack of heating flux into the loop, neither to the temporal characteristics of the heating, as shown by Antiochos et al. (1999), Mendoza-Briceño et al. (2002), Müller et al. (2003), and Müller et al. (2004). Rather it is linked to a specific spatial distribution of the heating, namely, basal heating. Only heating mechanisms having such heating scale heights allow catastrophic cooling to happen, thus pointing to the important link between coronal rain and coronal heating. Along these lines, Antolin et al. (2010) showed that if Alfvén wave heating is predominant in the loop, coronal rain is inhibited due to the characteristic uniform spatial heating ensuing from Alfvén waves.

High resolution observations in the last decade have unveiled a new important aspect of prominences: their thread-like structure (Heinzl & Anzer 2006; Lin et al. 2005, 2008; Lin 2010). At these ultra-small scales, prominences are observed to be composed of a myriad of fine threads (widths on the order of 200 km or less), outlining a fine-scale structure of the magnetic field. This magnetic field correspondence is further evidenced by the presence of flows along these threads (Martin et al. 2008). Although the prominence as a whole is a long-lived and rather static structure, the observed thread-like components appear to be very dynamic and short-lived (1–10 minutes). Likewise, very

high resolution observations of coronal rain with *Hinode*/SOT have shown strand-like structures with widths below 200 km (Antolin et al. 2010) traced by the condensations separating and elongating during their fall.

The detection of coronal rain requires therefore very high resolution observations. In this work we present such observations and perform a statistical study of velocities, accelerations, and falling angles of coronal rain observed with CRISP at the SST and SOT on *Hinode*. The CRISP spectropolarimeter allows us to obtain a more precise picture on the dynamics since it provides us with Doppler information, additionally to imaging. The obtained velocities are well below free fall, as has been reported in the past for prominences as well (Schrijver 2001; Zirker et al. 1994; Mackay & Galsgaard 2001). This accounts for the presence of other forces than gravity inside loops, most likely of magnetic origin, which may be related to the forces supporting prominences. The shapes of the falling condensations offer further evidence of very thin thread-like structures. Dynamics and shapes offer constraints on the nature of the forces inside the loops to which coronal rain is subject.

Waves have been observed frequently along prominences (Ramsey & Smith 1966; Oliver & Ballester 2002; Okamoto et al. 2007; Lin 2010) and coronal loops (Nakariakov & Verwichte 2005; Banerjee et al. 2007; Ruderman & Erdélyi 2009; Taroyan & Erdélyi 2009), leading to the determination of the internal physical conditions through the development of analytical and numerical modeling, thus spawning a very active research community in the field of prominence seismology. In this work, we also present the first observational analysis of transverse oscillations of threads in a loop, put in evidence by coronal rain. Strand-like condensations composing coronal rain are found to oscillate in phase, indicating transverse waves, probably of a collective nature. Periods, amplitudes, transversal velocities and phase speeds of the waves, as well as the coronal magnetic field, are estimated. We illustrate through this observational result the potential that coronal rain can have in the field of coronal seismology.

## 2. Observations with SST/CRISP and *Hinode*/SOT

The observations with CRISP (Scharmer et al. 2008) at the SST (Scharmer et al. 2003) were done in the spectral window  $[-0.12, 0.12]$  nm centered in  $H\alpha$ , on May 10, 2009 from 08:50 to 09:37 UT with a cadence of 6.4 s and a resolution of  $0''.0592 \text{ pixel}^{-1}$ , focusing on the active region (AR) 11017 on the east solar limb. The observations with *Hinode*/SOT (Tsuneta et al. 2008) were done in the Ca II H band on November 9, 2006 from 19:33 to 20:44 UT with a cadence of 15 s and a resolution of  $0''.05448 \text{ pixel}^{-1}$ , and focused on NOAA AR 10921 on the west limb. A statistical study focusing on the coronal rain observations by *Hinode*/SOT has already been done in Antolin et al. (2010). The statistical study presented here concentrates on the observations by CRISP.

In Fig. 1 we present a snapshot of the coronal rain falling down along a system of loops observed by CRISP of SST in  $H\alpha + 0.03$  nm. In color we plot the Doppler velocities derived by the spectropolarimeter over some of the loops exhibiting coronal rain. A radial filter which enhances the intensity of features above the limb has also been applied to the image. By tracing the falling condensations composing coronal rain we have calculated the velocities (projected and Doppler velocities), accelerations, and falling angles (with respect to the vertical) for a total of 235 condensations tracing 22 strands in total. This is shown in the histogram panels of Figure 2. As the condensations fall in general with non-constant velocities, we have measured the velocity

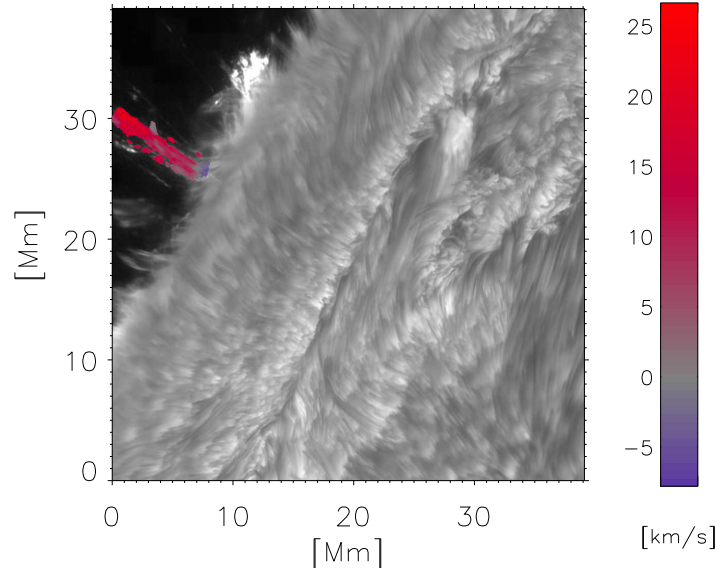


Figure 1. Coronal rain observed with CRISP in  $H\alpha + 0.03$  nm on May 10, 2009 above AR 11017. We plot in color the Doppler velocities for a loop with coronal rain.

for each condensation at two different heights, one high in the corona and another one towards the footpoints in the chromosphere, thus leading to an estimate of their acceleration, which we plot in the middle panel of the figure. However, only 76 out of the 235 condensations could be followed clearly along the strands. The rest of the condensations can mostly be discerned towards the footpoints. In the velocity panel on the left of Fig. 2 we have considered all the measurements, irrespective of their location along the strands. The velocities correspond to the total velocities, namely, the magnitude of the vector sum of the projected velocities in the plane of the sky (perpendicular to the line of sight) and the Doppler velocities. From these two components of the velocity we can calculate the angle at which the condensations fall with respect to the vertical. The histogram for the calculated angles is shown in the right panel of Figure 2. In all 3 panels, the dashed line corresponds to the mean values,  $70 \pm 23$  km s<sup>-1</sup>,  $0.12 \pm 0.17$  km s<sup>-2</sup>, and  $13.4 \pm 10^\circ$ , respectively, with their standard deviations.

In Fig. 3 we present the observations by *Hinode/SOT*. In the left panel we show a subset of the entire field of view, in which we plot the variance of the image over the period of time when coronal rain falls along the loop (about 15 minutes). We can see that the plane of the loop is roughly directed along the line of sight. The coronal rain in this case can be observed basically from the apex of the loop, located  $25 \pm 5$  Mm above the surface, leading to a loop length of  $80 \pm 15$  Mm assuming a circular loop. The dynamics of the condensations are similar to those observed by the SST and reported here (Antolin et al. 2010). The condensations separate and elongate, thus tracing several strands in the loop, and put in evidence in-phase transverse oscillations of the strands. This is shown in the right panel of Figure 3. Here we show the time slice along the outlined loop, where the transverse length refers to the perpendicular distance to the dotted line from dashed line to dashed line. At least 9 oscillation patterns can be clearly observed, over which we plot in color the (projected) distance where they

Table 1. Mean periods, amplitudes and transversal velocities for the 9 oscillatory events detected by *Hinode*/SOT on November 9, 2006 in a loop with coronal rain. Phase speeds and coronal magnetic fields are estimated according to the text.

Event	Period [s]	Amplitude [Mm]	Transversal velocity [km s <sup>-1</sup> ]	Phase speed [km s <sup>-1</sup> ]	Magnetic field [G]
1	112 ± 29	245 ± 148	4.5 ± 2.5	760 ± 265	16 ± 5.5
2	171 ± 11	515 ± 135	6.1 ± 1.4	460 ± 30	9.7 ± 0.6
3	118 ± 15	308 ± 136	5.3 ± 1.3	675 ± 90	14.2 ± 1.9
4	143 ± 17	324 ± 125	4.4 ± 1.2	555 ± 65	11.6 ± 1.4
5	165 ± -	351 ± 55	4.2 ± 0.1	475 ± -	10 ± -
6	198 ± 49	371 ± 205	3.6 ± 2.0	410 ± 90	8.6 ± 1.9
7	172 ± 20	406 ± 179	4.2 ± 1.0	460 ± 60	9.6 ± 1.2
8	176 ± 23	369 ± 255	3.8 ± 2.7	450 ± 60	9.5 ± 1.2
9	84 ± 8	305 ± 119	7.6 ± 4.0	940 ± 95	19.7 ± 2

happen from the apex of the loop. The in-phase oscillation can be observed in strands 1, 2, 3, 4, and 6 between the time period [15, 22] min in the figure. These strands become all visible simultaneously at roughly 8 Mm from the apex. The estimated periods, amplitudes, transversal velocities are shown in Table 2, as well as estimations for phase speeds and coronal magnetic fields according to the wave interpretation (see the next section).

### 3. Discussion

#### 3.1. Statistics of Coronal Rain from CRISP Observations

The coronal rain observed at the limb with the SST falls down roughly perpendicular to the solar surface. As shown in Fig. 1, CRISP indicates that most of the condensations are redshifted. Furthermore, the Doppler velocity of the condensations is observed to decrease with height above the solar surface. These facts fit in a scenario in which the loops have their planes roughly directed along the line of sight, with their farthest legs present in the field of view of the SST.

The observed coronal rain has a broad distribution of velocities, as shown in the left panel of Figure 2. This broadness comes not from a uniform acceleration of initially slowly falling condensations under the action of an effective gravity along the loops, but is the result of varying acceleration and deceleration processes. Indeed, the histogram in the middle panel of the figure shows an important spreading of accelerations, reaching even negative values indicating deceleration processes. As the mean of the distribution of the accelerations indicates,  $0.12 \pm 0.17 \text{ km s}^{-2}$ , almost all values are below the solar gravity value. Assuming nonetheless that the effective gravity (component along the loop) plays the main role in the dynamics of the condensations, the obtained mean value for the acceleration would be the result of falling at a mean angle of  $65^\circ$ . However, the inferred falling angles from the observed velocity components are almost all below  $30^\circ$ , as shown in the right panel of the figure. In fact, most of the observed heights for the condensations are between 10 and 20 Mm. Correlating the observed heights with the falling angles and assuming circular loops we obtain a best fit for the heights of the

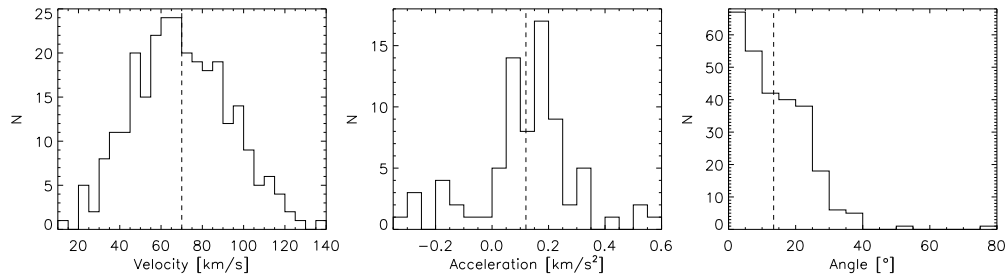


Figure 2. Histograms of velocity (*left*), acceleration (*middle*) and falling angle with respect to vertical (*right*) for the coronal rain observed with CRISP in Figure 1.

loop apices of  $38 \pm 13$  Mm, leading to total lengths of  $120 \pm 40$  Mm, which indicates that the observed part of the loops corresponds only to the lower legs.

In both SST and *Hinode* observations the condensations composing coronal rain are often observed to separate as they fall, resulting in elongation processes leading to thin thread-like structures of 200 km or lower. Thus, coronal rain in high resolution images is often observed to track strand-like structures within coronal loops. Whether the separation and elongation processes are just a result of gravity acting differentially along the magnetic topology or if other more sophisticated processes are involved is an interesting question that needs to be addressed properly with the help of numerical simulations. For instance, since the condensations appear to have chromospheric-like densities, thus becoming optically thicker, the local plasma beta parameter could be high enough to allow the plasma in the condensation to move transversally to the loop axis, thus allowing the separation of the initial dense blob.

### 3.2. Transverse MHD waves in coronal loops highlighted by coronal rain

The data set obtained by *Hinode*/SOT has become famous among solar limb observations. This is due mainly to the presence of an active region prominence which exhibits interesting oscillatory behavior. The waves running through this prominence were first interpreted as Alfvén waves (Okamoto et al. 2007), although various arguments have been put forward for an interpretation in terms of fast kink modes (Van Doorselaere et al. 2008; Terradas et al. 2008). The reported mean periods for the waves are between 130 and 240 s, (horizontal) oscillation amplitudes between 400 and 1770 km, transverse (vertical) velocities between 5 and  $15 \text{ km s}^{-1}$  and an estimated wave speed of  $> 1050 \text{ km s}^{-1}$  leading to a magnetic field of 50 G in the prominence.

Additionally, on the foreground of the prominence various loops exhibiting coronal rain have been observed (Antolin et al. 2010). In one of these loops, located on the south side of the *Hinode*/SOT field of view (right hand side of Figure 1 in that paper, left panel in Figure 3 here) transverse oscillations are put in evidence by the coronal rain. Several strand-like condensations are observed to oscillate in-phase, which points to a transverse wave affecting the loop as one structure, rather than being random local perturbation processes in the strands. The oscillations can not only be confined to the loop but can involve a larger coronal region, and thus could be related to the oscillations reported by Okamoto et al. (2007) present in the background prominence. The periods are similar but the amplitudes are somewhat smaller in our case, and more importantly,

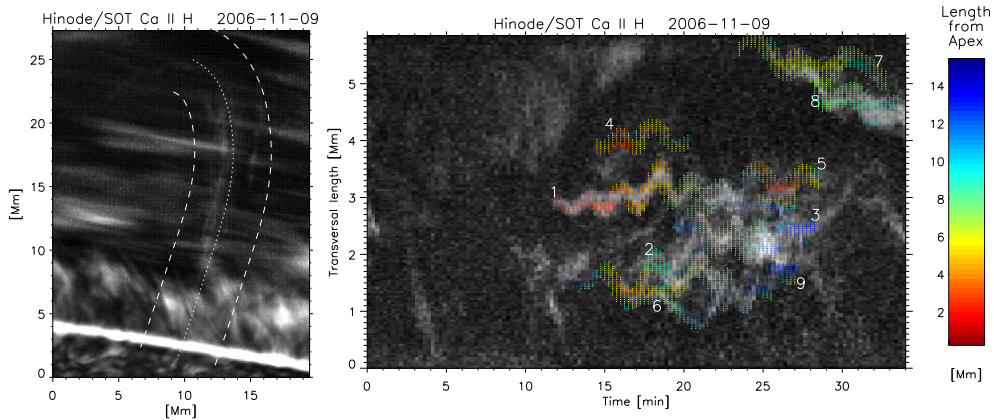


Figure 3. *Left:* Loop with coronal rain observed by *Hinode/SOT* on November 9, 2006 above AR 10921. *Right:* Time slice across the loop (transversal width corresponds to width of the loop delimited by the dashed lines in the left panel) for the time interval when coronal rain is observed. 9 oscillations can be detected. We plot in color over the oscillations the length from the apex where they occur.

the oscillation is along the horizontal plane, whereas the oscillation in the prominence is along the vertical plane. Furthermore, the loops on the north side of the sunspot (analyzed in Antolin et al. 2010) do not exhibit oscillatory motions.

Since the oscillations in the loop can only be observed when the condensations are falling it is not clear whether the agent is a propagating or a standing wave. The condensations do not appear to be oscillating when they are at the apex of the loop (as shown for instance by strand 1 in Fig. 3) and the amplitudes indicate a maximum at roughly halfway along the loop leg (one fourth of the total loop length), which correspond to signatures of the first harmonic of a standing mode. On the other hand, we could think of a propagating wave packet, propagating up or down, the maximum amplitude meeting the condensations half way through the loop's leg. Although the latter scenario is less likely, it cannot be excluded.

In the case of a first harmonic, the total wavelength is equal to the loop length, i.e.  $\approx 80$  Mm, leading to phase speeds between 400 and 1000 km s<sup>-1</sup> (see Table 2). If we assume that the density inside the loop is quite higher than the density outside the loop (as expected from catastrophic cooling loops), we would be assuming the presence of a waveguide along the loop, in which case the wave causing the oscillations would be a fast kink wave. Taking a typical density ratio of 0.1 between outside and inside densities, assuming a loop number density of  $3 \times 10^9$  cm<sup>-3</sup>, a rough maximum limit of dense loops subject to catastrophic cooling (Antolin et al. 2010) and using formula 31 in Nakariakov & Verwichte (2005) (corrected for the first harmonic), we obtain a coronal magnetic field in the loop between 9 and 20 G. It is important to note, however, that the condensations do not oscillate in-phase throughout the entire falling time. The loss of phase may be a signature of a non-collective character of the wave. A torsional Alfvén wave is known to exhibit such behavior due to phase mixing.

The causes of such oscillation are less clear. The most natural scenario is one in which the waves are generated at photospheric level by magnetic reconnection. We can

also think of a special case in which coronal rain itself leads to a kink mode in the loop, a scenario worthy of investigation through numerical simulations.

**Acknowledgments.** P.A. would like to thank the SOC and LOC for the opportunity to present this work.

## References

- Antiochos, S. K., MacNeice, P. J., Spicer, D. S., & Klimchuk, J. A. 1999, *ApJ*, 512, 985
- Antolin, P., Shibata, K., & Vissers, G. 2010, *ApJ*, 716, 154
- Aschwanden, M. J. 2001, *ApJ*, 560, 1035
- Banerjee, D., Erdélyi, R., Oliver, R., & O’Shea, E. 2007, *Solar Phys.*, 246, 3
- De Groof, A., Berghmans, D., van Driel-Gesztelyi, L., & Poedts, S. 2004, *A&A*, 415, 1141
- De Pontieu, B., McIntosh, S. W., Carlsson, M., Hansteen, V. H., Tarbell, T. D., Boerner, P., Martínez-Sykora, J., Schrijver, C. J., & Title, A. M. 2011, *Science*, 331, 55
- Hara, H., Watanabe, T., Harra, L. K., Culhane, J. L., Young, P. R., Mariska, J. T., & Doschek, G. A. 2008, *ApJ*, 678, L67
- Heinzel, P., & Anzer, U. 2006, *ApJ*, 643, L65
- Kawaguchi, I. 1970, *PASJ*, 22, 405
- Leroy, J.-L. 1972, *Solar Phys.*, 25, 413
- Lin, Y. 2010, *Space Sci. Rev.*, 112
- Lin, Y., Engvold, O., Rouppe van der Voort, L., Wiik, J. E., & Berger, T. E. 2005, *Solar Phys.*, 226, 239
- Lin, Y., Martin, S. F., & Engvold, O. 2008, in *Subsurface and Atmospheric Influences on Solar Activity*, edited by R. Howe, R. W. Komm, K. S. Balasubramaniam, & G. J. D. Petrie, vol. 383 of *Astronomical Society of the Pacific Conference Series*, 235
- Mackay, D. H., & Galsgaard, K. 2001, *Solar Phys.*, 198, 289
- Martin, S. F., Lin, Y., & Engvold, O. 2008, *Solar Phys.*, 250, 31
- Mendoza-Briceño, C. A., Erdélyi, R., & Di G. Sigalotti, L. 2002, *ApJ*, 579, L49
- Müller, D. A. N., Hansteen, V. H., & Peter, H. 2003, *A&A*, 411, 605
- Müller, D. A. N., Peter, H., & Hansteen, V. H. 2004, *A&A*, 424, 289
- Nakariakov, V. M., & Verwichte, E. 2005, *Living Reviews in Solar Physics*, 2, 3
- Okamoto, T. J., Tsuneta, S., Berger, T. E., Ichimoto, K., Katsukawa, Y., Lites, B. W., Nagata, S., Shibata, K., Shimizu, T., Shine, R. A., Suematsu, Y., Tarbell, T. D., & Title, A. M. 2007, *Science*, 318, 1577
- Oliver, R., & Ballester, J. L. 2002, *Solar Phys.*, 206, 45
- Ramsey, H. E., & Smith, S. F. 1966, *AJ*, 71, 197
- Ruderman, M. S., & Erdélyi, R. 2009, *Space Sci. Rev.*, 149, 199
- Scharmer, G. B., Bjelksjo, K., Korhonen, T. K., Lindberg, B., & Petterson, B. 2003, in *Innovative Telescopes and Instrumentation for Solar Astrophysics*, edited by S. L. Keil & S. V. Avakyan, vol. 4853 of *Society of Photo-Optical Instrumentation Engineers (SPIE) Conference Series*, 341
- Scharmer, G. B., Narayan, G., Hillberg, T., de la Cruz Rodríguez, J., Löfdahl, M. G., Kiselman, D., Sütterlin, P., van Noort, M., & Lagg, A. 2008, *ApJ*, 689, L69
- Schrijver, C. J. 2001, *Solar Phys.*, 198, 325
- Taroyan, Y., & Erdélyi, R. 2009, *Space Sci. Rev.*, 149, 229
- Terradas, J., Arregui, I., Oliver, R., & Ballester, J. L. 2008, *ApJ*, 678, L153
- Tsuneta, S., Ichimoto, K., Katsukawa, Y., Nagata, S., Otsubo, M., Shimizu, T., Suematsu, Y., Nakagiri, M., Noguchi, M., Tarbell, T., Title, A., Shine, R., Rosenberg, W., Hoffmann, C., Jurcevich, B., Kushner, G., Levay, M., Lites, B., Elmore, D., Matsushita, T., Kawaguchi, N., Saito, H., Mikami, I., Hill, L. D., & Owens, J. K. 2008, *Solar Phys.*, 249, 167
- Van Doorselaere, T., Nakariakov, V. M., & Verwichte, E. 2008, *ApJ*, 676, L73
- Zirker, J. B., Engvold, O., & Yi, Z. 1994, *Solar Phys.*, 150, 81